

Bolometric Light Curves of Supernovae

Nicholas B. Suntzeff

Cerro Tololo Inter-American Observatory, National Optical Astronomy Observatories,
Casilla 603, La Serena, Chile

Abstract. The thermalized energy from the radioactive decays of ^{56}Ni and ^{57}Ni and their daughter nuclides power the light curves of supernovae near maximum light. The bolometric light curve gives us a fundamental understanding of the energy evolution of a supernova explosion and the amount of radioactive nuclides produced. In this review, I will discuss the bolometric evolution of the Type IIp supernovae SN1987A, and the general class of bolometric light curves of Type Ia thermonuclear explosions.

1 SN1987A

We have been monitoring the photometric properties of the Type IIp SN1987A in the LMC for more than 15 years. Over the first 5 years the optical photometry could be measured from the ground in the typical 1" seeing at our observatories. In the near infrared bands of *JHK* where the seeing is better and the crowding stars (which are typically bluer than the SN) are less of a problem, we could monitor the SN for up to 10 years. Once the supernova faded below the integrated magnitudes of the inner ring which lies at about 1" from the supernova debris, *HST* or ground-based AO imagery is needed to isolate the debris and inner ring evolution. In Figure 1, I show the structure of the inner ring region.

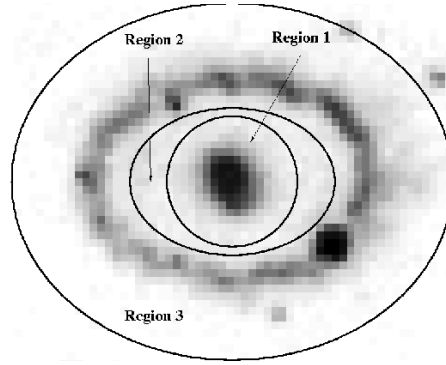


Fig. 1. An *HST* image of region near the inner ring of SN1987A. Region 1 isolates the expanding debris. Region 2 represents the shocked region between the debris and the inner ring. Region 3 represents the inner ring

From our *HST* images, we have measured the evolution of the brightness of the three regions shown in Fig. 1 with respect to an averaged background region outside of Region 3. For the earlier ground-based data where we can only measure the light from all three regions, we have subtracted off the extrapolated flux from Regions 2 and 3 to derive estimated fluxes for just the debris region. In Fig. 2 we plot the optical light curve for 15 years of evolution. With these corrections, the optical and *HK* photometry from the ground and *HST* flight system equivalents merge well together. The near-infrared photometry in *J/F110W* shows a large discontinuity presumably due to the radical differences in the two filter systems. The photometry of non-stellar SEDs can show large systematic errors due to the differences in the sensitivity functions of the atmosphere/telescope/filter/detector system. In early photometry of SN1987A, we noted difference of up to 0.4 mag in *I* photometry due to the differences in the facility *I* filters [1]. In Table 1, I list the latest photometry for SN1987A

Table 1. Optical Photometry of SN1987A as of May 2002

	<i>U</i>	<i>B</i>	<i>V</i>	<i>R</i>	<i>I</i>
debris	20.91(32)	20.88(12)	21.28(07)	20.96(22)	20.46(04)
decay rate (mag y ⁻¹)	0.23	0.20	0.24	0.35	0.22

Table 2. Near-Infrared Photometry of SN1987A

days since explosion	<i>J</i>	<i>H</i>	<i>K</i>
4151	19.81(09)	18.29(06)	18.40(02)
5428	20.46(15)

The leveling off of the light curves after year 5 is due to two causes: the longer decay times for the remaining radioactive nuclides and the freeze-out of the cooling. By year five, the main radioactive energy sources of ⁵⁶Ni and its daughter nucleus ⁵⁶Co with e-folding times of 8.8d and 111.3d have decayed away. The nuclides ⁵⁷Co (the daughter nuclide of ⁵⁷Ni) and ⁴⁴Ti with e-folding times of 390d and 87y are left as the main energy input, along with the energy input from a possible (but as yet unseen) pulsar. However, the light curves at this phase no longer represent the prompt thermalization of the input radioactive energy. As shown in [2,3], the recombination and cooling time scales become larger than the expansion time scale, and the debris nebula is not able to cool at the rate of radioactive energy input.

The ultraviolet, optical, and infrared photometry can be integrated to the thermalized “uvoir” energy flux to derive the masses of the synthesized radioactive nuclides. The early time data (less than 1000d) with prompt thermalization

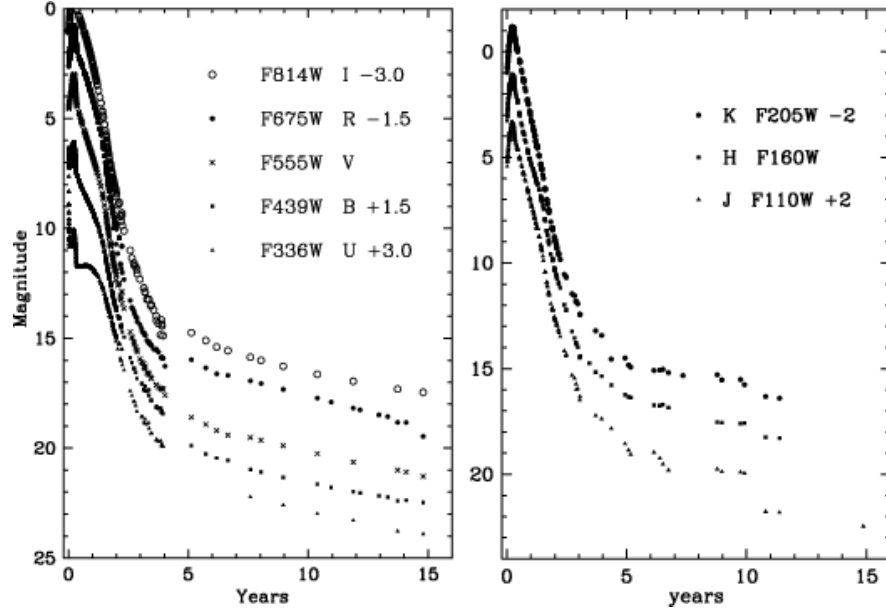


Fig. 2. Optical light curves (left panel) and near-infrared light curves (right panel) for the debris (Region 1) in SN1987A. The data have been shifted by the magnitudes listed in the legend. The data are a combination of ground-based *UBVR**IJK* and the equivalent *HST* flight system magnitudes.

and cooling can be simply fit to radioactive decay models as in [4,5,6]. The late-time bolometric light curves, when fit with models including the freeze-out, can be used to measure the amount of ^{57}Ni and ^{44}Ti . Fransson and Kozma ([3]) present the latest values for the amounts of these nuclides where they found the following masses: $M(^{57}\text{Ni}, ^{57}\text{Ni}, ^{44}\text{Ti}) = (0.069, 0.003, 0.0001)M_{\odot}$. Lundqvist et al. ([7]) find upper limits on the mass of ^{44}Ti consistent with these numbers based on the non-detection of the $25\text{m}\mu$ lines of [FeI] and [FeII] from ISO/SWS. They caution, however, that if dust cooling is important, the limits on the mass of ^{44}Ti could be significantly higher. Only direct detection of the 1.157 MeV line of ^{44}Ti will resolve the ambiguity in the models.

In Fig. 3 I show the late-time photometric data for the ring and the inter-ring region. The ring region suddenly began to brighten at a rate of $\sim -0.24 \text{ mag y}^{-1}$ in *UBVI* and $\sim -0.12 \text{ mag y}^{-1}$ in *R* since year 13. The brightening of the ring was predicted in [8,9,10]. The ring was expected to brighten by 7.5mag to about $V = 11$ as the blast wave from the debris struck the inner ring starting around year 16-20. However, in year 10, Pun et al. ([11]) discovered a single spot brightening, evidently due to an inward protrusion of the inner ring. Our observations here show that the general rapid brightening of the ring began later, around year 13.

The inter-ring region has accelerated its brightening since year 13 and is now brightening at a rate of $\sim -0.12 \text{ mag y}^{-1}$ in *UBVI*. The inter-ring light is presumably due to the emission from the reverse shock which is located at $\sim 75\%$ of the radius of the inner boundary of the inner ring. This emission was predicted by [10] and discovered by [12] with STIS data from *HST*. Refined models are presented in [13,14]. The reverse shock formed in the equatorial plane as neutral hydrogen atoms streaming from the debris at 15000 km s^{-1} hit the ionized region at the inner surface of the ring. There is also diffuse light present in the STIS data which may be due to excitation by non-thermal particles accelerated by the shock.

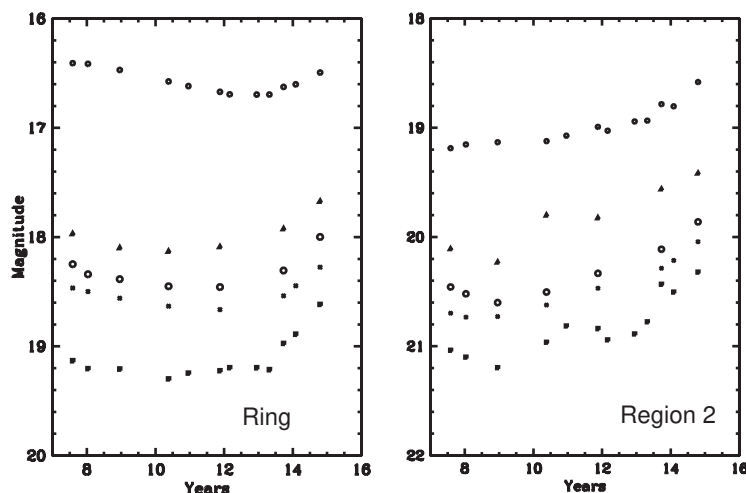


Fig. 3. *UBVR* optical light curves for the ring Region 3 (left panel) and the inter-ring Region 2 (right panel). The magnitudes from bottom to top are *BVIUR*.

Significant dust formed in SN1987A starting around day 500, and by day 1000, the bolometric flux of the nebula was dominated by dust radiation with a temperature of $T_{dust} \sim 200\text{K}$ and mid-infrared line emission([6,15]). In Fig. 4 I show the latest data on the mid-infrared evolution of SN1987A with the ISO-CAM detection ([16]) and a detection from OSCIR on the CTIO 4m telescope ([17]) at $10\mu\text{m}$. Without $20\mu\text{m}$ detections however, we can't estimate the dust temperature and cannot measure the dust emission. If we assume the same bolometric corrections from day 1800, we find the bolometric flux of SN1987A is $\log_{10}(L) \sim 36.0 \text{ erg s}^{-1}$.

2 The Bolometric Behavior of Type Ia Supernovae

Because there is much less envelope mass above the radioactive energy sources in Type Ia SNe, the bolometric properties of these supernovae are more difficult

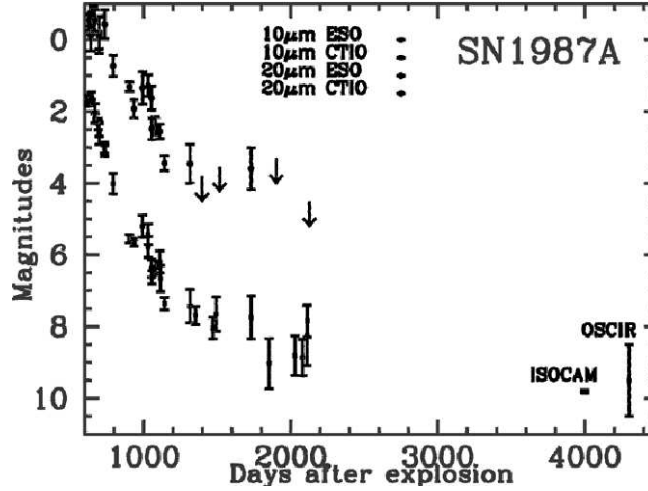


Fig. 4. Mid-infrared light curves of SN1987A

to interpret because much less of the radioactive energy is thermalized. The physics of the thermalization is discussed in [18,19]. The fraction of the radiation which is thermalized must be transported to the surface and radiated away. If the diffusion time for the energy is short compared to the dynamical time, the energy appears as thermalized “uvoir” radiation. If the diffusion time is long, the trapped radiation will be converted partly into kinetic energy and not seen in the bolometric light curve. With a longer diffusion time, the peak of the bolometric light curve is shifted to later times when the input energy from the radioactive decays is less. This leads to “Arnett’s Law” [23] which states that the bolometric luminosity at maximum light is equal to the instantaneous energy released by the radioactive decay. This law was (and is) an important tool to measure the amount of radioactive nickel produced in the explosion.

Continuing the discussion in [18], for the first 60 days since explosion the thermalization time is short compared to the dynamical time, and little radioactive energy is converted into kinetic energy. Thus the integrated uvoir bolometric luminosity represents the fraction of radioactive energy input which has been thermalized. By day 40 more than one half of gamma-ray radiation is leaving the explosion unthermalized. Even at B maximum light some 20 days after explosion, some 15% of the gamma rays are unthermalized. The observed uvoir bolometric light curve is then a function of the rapidly decreasing optical depth to the gamma-rays over the first 100 days and the decreasing energy input from the radioactive nickel nuclides. The combination of these two processes accelerates the light curve decay at a rate faster than the radioactive decay of ^{56}Co after maximum light.

The uvoir bolometric light curve interpretation is also complicated by the efficiency of the trapping of the gamma rays and positrons in the ^{56}Co decay

([20,21,22]). Milne et al. ([21]) show that the gamma-rays from the ^{56}Co decay carry 30 times more energy than the positrons, but also are more penetrating and can escape more easily. As the nebula expands from days 50 to 200, the energy deposition switches from the ^{56}Co gamma-ray Comptonization to the energy input from the positron annihilations. Some of the positrons, however, can be transported out of the nebula, depending on the magnetic fields structure. The bolometric light curve at this phase then becomes dependent on the details of the mixing of the ^{56}Co in the nebula and the properties of the magnetic fields.

While the interpretation of the bolometric light curve requires theoretical knowledge of the optical depths to gamma-rays and the details about the mixing of ^{56}Ni , the construction of the uvoir bolometric light curve is rather simple due to the following coincidence - - *most of the thermalized flux appears at optical wavelengths*. In Fig. 5 I show the cumulative flux of SN1992A at various phases during the first 100 days of evolution ([24]). Also shown in the figure is a comparison of a Type Ia SED with that of a Type Ic and II ([25,26]). It can be clearly seen that the broad peak of the flux distribution for Type Ia SNe appears in the optical region. In fact, typically 80% or more of the uvoir flux appears in the optical from day -6 onwards.

Only a few papers have been published trying to estimate the bolometric light curves (see [22] for a summary). In [27,28], the optical broad-band magnitudes were integrated to provide a magnitude that should be a close surrogate to the uvoir bolometric magnitude. From the estimated bolometric light curve, they found a range of more than a factor in 10 in the ^{56}Ni masses for a group of nearby Type Ia SNe. In [29], a V magnitude was used with a bolometric correction to study the gamma-ray trapping in the late-time light curves, which also showed a significant range in ^{56}Ni masses.

In 1996, I used the small amount of data on supernovae which had space ultraviolet spectra, optical $UBVRI$, and near-infrared JHK data to estimate accurate bolometric fluxes ([24]). I found that there was a range in peak bolometric magnitudes (implying a range in nickel masses) and that the bolometric light curves appear to have a small secondary hump in the light curve around days 20-40 corresponding to the secondary maximum in the I band. Such a flux redistribution was unexpected, and points to a rather sudden change in the opacity and cooling in the nebula.

The construction of the bolometric light curve requires the sum of the space ultraviolet, optical, and near-infrared data. The falloff of the flux beyond H is such that the assumption of a R-J law adds only a few percent to the total flux and a R-J extrapolation from H or K is entirely adequate. The extrapolation to the space ultraviolet, however, is larger. Using 1992A data, I found that extrapolating the U flux point at 360nm to zero flux at 300nm was a reasonable representation of the true space ultraviolet flux from day -6 onwards, yielding agreement to 5% in the uvoir flux between the full integration and the integration using the ultraviolet extrapolation. It is important to continue to observe nearby SNe with HST in the ultraviolet to understand the diversity of the ultraviolet flux, which may be an indicator of the metallicity of the progenitor.

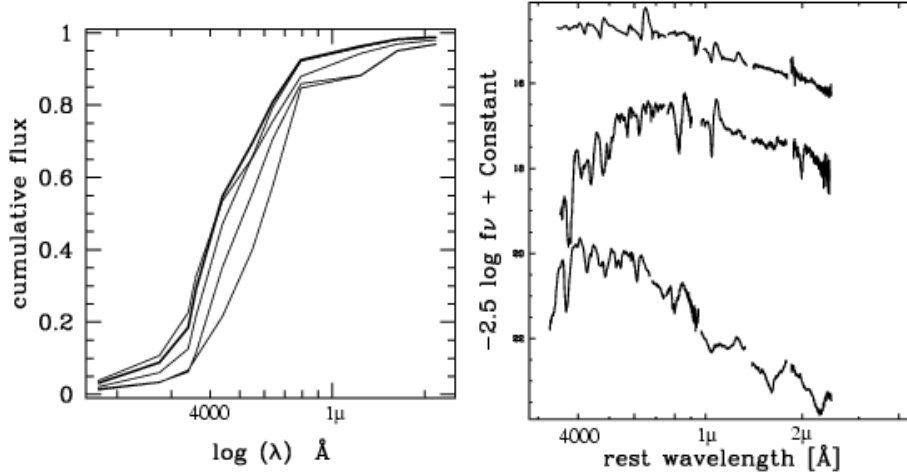


Fig. 5. Flux distributions of Type Ia SNe. The left panel shows the cumulative flux distribution for SN1992A for days $-6, 0, 5, 20, 80$ (from top to bottom at $\lambda = 300\text{nm}$), with the distribution for day 0 shown in the darker line. 80% or more of the total uvoir flux appears in the optical window of $300\text{-}1000\text{nm}$. The right panel shows the SEDs (top to bottom) for SN1999em (Type II), SN 1999ex (Ibc) and SN 1999ee (Type Ia) near maximum light (reference [25]). Note that the broad flux peak of the SED appears in the optical.

Our groups at CTIO and LCO have been following nearby Type Ia and Type II in *UBVRIYJHK* in part to study the bolometric properties of these supernovae. The new filter *Y* at $1\mu\text{m}$ ([30]) has been designed to fit in a wavelength band which is remarkably free of telluric absorption and provides a flux point between the widely separated *I* and *J* filters. Figure 6 ([31]) shows the SED evolution of the nearby SN 2001el. This figure shows that the SED is well fit by a black-body with $T_{eff} = 14,000\text{K}$ before maximum light steepening to a R-J law by maximum light in *BVRIJHK*. After maximum light, a flux deficit appears in *J* and the bands *UBV* drop away from a thermal distribution.

In Figure 7 I plot the uvoir bolometric light curves calculated from the integration of the broad-band magnitudes, including an extrapolation to the ultraviolet to account for the unobserved space ultraviolet, and to the infrared using a R-J law extending from *I* or *K*. The absolute flux scale has been set by using either SBF, Cepheid, TRGB, or PN distances for the nearby SNe, or a Hubble law of $H_0 = 74 \text{ km s}^{-1} \text{ Mpc}^{-1}$ for the more distant SNe. The comparison of SN1999ee and SN2001el shows that the location and size of the secondary bump is significantly different despite the fact that the peak luminosities are very similar.

Also plotted in Fig. 7 are the uvoir bolometric light curves for 16 Type Ia SNe. All have *UBVRI* photometry and 10 have *JHK* photometry. The sense of this figure is that most SNe have roughly the same peak bolometric luminosity,

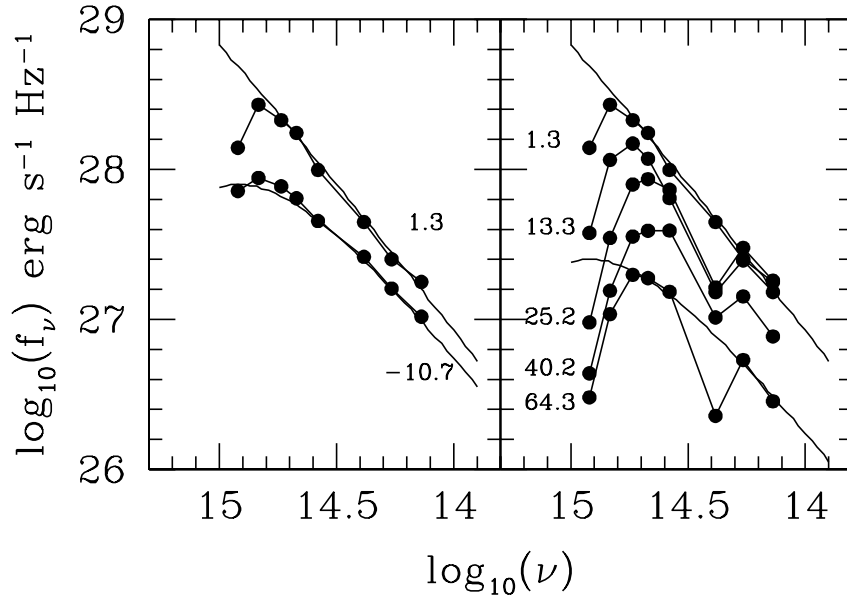


Fig. 6. SED evolution for the Type Ia SN2001el. The left panels shows the SEDs for days (since B_{max}) -10.7 and $+1.3$. The right panel shows the SEDs for days 1.3, 13.3, 25.2, 40.2, and 64.3. A $T_{eff} = 14,000\text{K}$ blackbody is fit to the -10.7 and 64.3 data, and a Rayleigh-Jeans law is fit to the data 1.3 data. The SED steepens to the blue as the SN approaches maximum light and then reddens after maximum. The flux deficit in J appears right after maximum light. Note that the IHK data roughly follow the R-J law.

but the size and placement of the secondary hump is quite variable. For instance, the peculiar SN2000cx has a rather normal bolometric light curve near maximum light, but almost completely lacks a secondary hump at 30 days. This bolometric behavior reflects the fact that SN2000cx had an anomalously weak I -band secondary maximum. Evidently the peak bolometric magnitude (and thus the ^{56}Ni mass) is not strongly coupled to the opacity and flux redistribution causing the secondary hump.

Finally, in Fig. 8 I show the peak bolometric luminosity versus the light curve shape parameter Δm_{15} for the sample plotted in Fig. 7. Rather than the roughly linear relationship between the intrinsic luminosity in B or V and Δm_{15} , we find that for much of the range of Δm_{15} there is little or no relationship between $\log_{10}(L)$ at peak and Δm_{15} , at least for $\Delta m_{15} < 1.3$.

Acknowledgments: I would like to thank my collaborators: M. Phillips and M. Hamuy (LCO); P. Bouchet, P. Candia, K. Krisciunas, R. Schommer (deceased 12 December 2001), and C. Smith, (CTIO); B. Leibundgut (ESO); R. Kirshner, P. Challis and the SInS collaboration; and B. Schmidt (MSSSO) and the

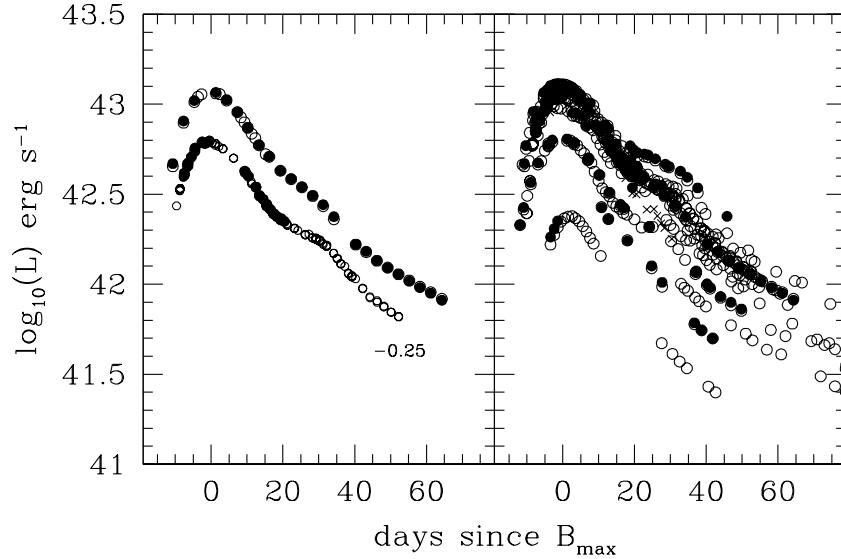


Fig. 7. “UVOIR” bolometric light curves for Type Ia SNe. These light curves include extrapolations to the space ultraviolet and the extrapolation to the red using a R-J law. Closed circles indicate an extrapolation from K and open circles indicate an extrapolation from I . The left panel shows the bolometric light curves for SN2001el (upper curve, $\Delta m_{15} = 1.13$) and SN1999ee (lower curve, $\Delta m_{15} = 0.94$). The SN1999ee data have been shifted by 0.25dex for presentation purposes. The right panel shows the bolometric light curves for 16 Type Ia SNe.

High-Z Supernova Team for their help in the collection of these data. This research was supported in part by HST grants GO-07505.02A, GO-08177.6, and GO08641.07A.

References

1. N. Suntzeff, et al.: *Astron. J.*, **117**, 1175 (1988)
2. C. Fransson, C. Kozma *Astroph. J. Lett.*, **408**, L25 (1993)
3. C. Fransson, C. Kozma: *New Astronomy Review*, **46**, 487 (2002)
4. N. Suntzeff, P. Bouchet: *Astron. J.*, **99**, 650 (1990)
5. P. Bouchet et al.: *Astron. Astroph.*, **245**, 490 (1991)
6. N. Suntzeff, et al.: *Astroph. J. Lett.*, **384**, L33 (1992)
7. P. Lundqvist et al.: *Astron. Astroph.*, **374**, 629 (2001)
8. D. Lou, R. McCray: *Astroph. J.*, **379**, 659 (1991)
9. R. Chevalier, V. Dwarkadas: *Astroph. J. Lett.*, **452**, L45 (1995)
10. K. Borkowski, J. Blondin, R. McCray: *Astroph. J. Lett.*, **476**, L31 (1997)
11. C. Pun, et al.: *IAU Circ.* 6665 (1997)
12. G. Sonneborn, et al.: *Astroph. J. Lett.*, **492**, L139 (1998)

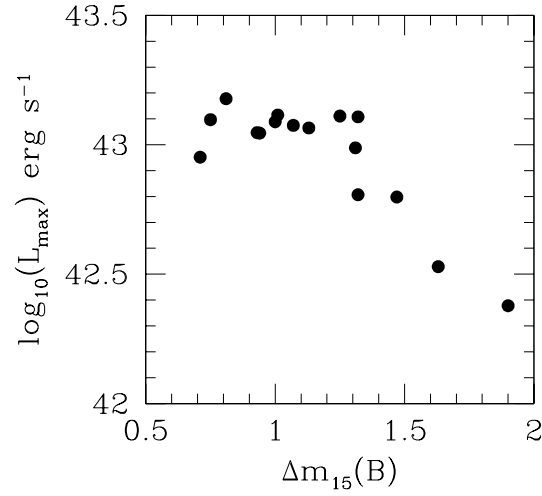


Fig. 8. The peak uvoir bolometric luminosity plotted against the light curve shape parameter of [32] for the SNe shown in Fig. 7.

13. E. Michael, et al.: *Astroph. J. Lett.*, **492**, L143 (1998)
14. E. Michael, et al.: *Astroph. J. Lett.*, **509**, L117 (1998)
15. D. Wooden, et al.: *Astroph. J. Sup.*, **88**, 477 (1993)
16. J. Fischera, R. Tuffs, H. Völk: *Astron. Astrop.*, **386**, 517 (2002)
17. P. Bouchet: private communication (2002)
18. B. Leibundgut, P. Pinto 1992: *Astroph. J.*, **401**, 49 (1992)
19. B. Leibundgut: *Astron. Astrop. Rev.*, **10**, 179 (2000)
20. P. Ruiz-Lapuente, H. Spruit: *Astroph. J.*, **500**, 360 (1998)
21. P. Milne, et al.: *Astroph. J.*, **559**, 1019 (2001)
22. B. Leibundgut, N. Suntzeff: "Light Curves of supernovae" In *Supernovae & GRBs xxx*, ed. K. Weiler, (Springer-Verlag, xxx, 2003) in press
23. W. Arnett: *Astroph. J.*, **253**, 785 (1982)
24. N. Suntzeff: 'Observations of Type IA Supernovae'. In: *IAU Colloq. 145: Supernovae and Supernova Remnants*, ed. R. McCray, Z. Wang (Cambridge University Press, Cambridge 1996) pp41-51
25. M. Hamuy, et al.: *Astron. J.*, **124**, 417 (2002)
26. M. Hamuy, et al.: *Astron. J.*, **124**, 2339 (2002)
27. G. Contardo, B. Leibundgut, W. Vacca: *Astron. Astrop.*, **359**, 876 (2000)
28. W. Vacca, B. Leibundgut: *Astroph. J. Lett.*, **471**, L37 (1996)
29. E. Cappellaro, et al.: *Astron. Astrop.*, **328**, 203 (1997)
30. L. Hillenbrand, et al.: *PASP*, **114**, 708 (2002)
31. K. Krisciunas, et al.: *Astron. J.*, in press (astro-ph/0210327) (2003)
32. M. Phillips: *Astroph. J. Lett.*, **413**, L105 (1993)